TOXICOLOGICAL SCIENCES **91(1)**, 173–183 (2006)
doi:10.1093/toxsci/kfj127
Advance Access publication February 13, 2006

Distinct Cytotoxic Mechanisms of Pristine versus Hydroxylated Fullerene

Aleksandra Isakovic,* Zoran Markovic,† Biljana Todorovic-Markovic,† Nadezda Nikolic,† Sanja Vranjes-Djuric,† Marija Mirkovic,† Miroslav Dramicanin,† Ljubica Harhaji,‡ Nevena Raicevic,‡ Zoran Nikolic,§ and Vladimir Trajkovic[¶,1]

*Institute of Biochemistry, School of Medicine, University of Belgrade, 11000 Belgrade, Serbia and Montenegro; †Vinca Institute of Nuclear Sciences, 11000 Belgrade, Serbia and Montenegro; ‡Institute for Biological Research, 11000 Belgrade, Serbia and Montenegro; §Faculty of Physics, University of Belgrade, 11000 Belgrade, Serbia and Montenegro; and ¶Institute of Microbiology and Immunology, School of Medicine, University of Belgrade, 11000 Belgrade, Serbia and Montenegro

Received November 18, 2005; accepted February 1, 2006

The mechanisms underlying the cytotoxic action of pure fullerene suspension (nano-C_{60}) and water-soluble polyhydroxylated fullerene [$C_{60}(OH)_n$] were investigated. Crystal violet assay for cell viability demonstrated that nano-C_{60} was at least three orders of magnitude more toxic than $C_{60}(OH)_n$ to mouse L929 fibrosarcoma, rat C6 glioma, and U251 human glioma cell lines. Flow cytometry analysis of cells stained with propidium iodide (PI), PI/annexin V–fluorescein isothiocyanate, or the redox-sensitive dye dihydrorhodamine revealed that nano-C_{60} caused rapid (observable after few hours), reactive oxygen species (ROS)–associated necrosis characterized by cell membrane damage without DNA fragmentation. In contrast, $C_{60}(OH)_n$ caused delayed, ROS-independent cell death with characteristics of apoptosis, including DNA fragmentation and loss of cell membrane asymmetry in the absence of increased permeability. Accordingly, the antioxidant N-acetylcysteine protected the cell lines from nano-C_{60} toxicity, but not $C_{60}(OH)_n$ toxicity, while the pan-caspase inhibitor z-VAD-fmk blocked $C_{60}(OH)_n$-induced apoptosis, but not nano-C_{60}–mediated necrosis. Finally, $C_{60}(OH)_n$ antagonized, while nano-C_{60} synergized with, the cytotoxic action of oxidative stress–inducing agents hydrogen peroxide and peroxynitrite donor 3-morpholinosydnonimine. Therefore, unlike polyhydroxylated C_{60} that exerts mainly antioxidant/cytoprotective and only mild ROS-independent pro-apoptotic activity, pure crystalline C_{60} seems to be endowed with strong pro-oxidant capacity responsible for the rapid necrotic cell death.

Key Words: **cytotoxicity; fullerene; C_{60}; reactive oxygen species; apoptosis; necrosis.**

Water-soluble fullerene derivatives synthesized by attaching various functional groups (−OH, −COOH, $-NH_2$) to the fullerene cage (C_{60}) are promising candidates for many biomedical applications, including cytoprotection, DNA photocleavage, enzyme inhibition, diagnostic imaging, and antimicrobial and anticancer therapy (Bosi *et al.*, 2003). Due to electrochemical features that enable reaction with cell-damaging reactive oxygen species (ROS) such as superoxide ($O_2^{\bullet}-$) and hydroxyl ($^{\bullet}OH$) radicals, the fullerene core behaves as a free radical sponge with a protective effect in experimental ROS-dependent neuronal death, both *in vitro* and *in vivo* (Dugan *et al.*, 1997, 2001; Lotharius *et al.*, 1999). Polyhydroxylated fullerenes [$C_{60}(OH)_n$], also known as fullerols or fullerenols, are particularly efficient antioxidants, reducing ROS-mediated neuronal death induced by engagement of glutamate receptors (Dugan *et al.*, 1996; Jin *et al.*, 2000). Treatment with fullerols also afforded protection against oxidative stress in the RAW 264.7 macrophage cell line and ischemia-reperfused rat lungs (Chen *et al.*, 2004), and significantly reduced doxorubicin toxicity against human breast cancer cell lines (Bogdanovic *et al.*, 2004). On the other hand, fullerol itself caused RAW 264.7 cell death (Chen *et al.*, 2004) and suppressed proliferation of human breast cancer cells in a cell line–dependent manner (Bogdanovic *et al.*, 2004). The mechanisms responsible for the cytotoxic and cytostatic action of $C_{60}(OH)_n$ in these studies were not investigated, while its antiproliferative effect on rat vascular smooth muscle cells was apparently associated with inhibition of protein tyrosine kinase activity (Lu *et al.*, 1998).

Investigation of the biological properties of pure, underivatized fullerene has been greatly hampered by its complete lack of solubility in water. However, pure C_{60} can be brought into water by means of solvent extraction or simply by stirring over time, which results in formation of water-stable aggregates (Cheng *et al.*, 2004; Deguchi *et al.*, 2001). As the unintentional generation of these aggregates in aqueous environments is a possibility, their toxicological effects are of great importance, particularly if C_{60} finds widespread use in consumer products. Recently, Sayes *et al.* (2004) described the several orders of magnitude higher toxicity of pure C_{60} against human dermal fibroblasts and liver carcinoma HepG2 cells, in

[1] To whom correspondence should be addressed at Institute of Microbiology and Immunology, School of Medicine, University of Belgrade, Dr. Subotica 1, 11000 Belgrade, Serbia and Montenegro. Fax: +381 11 265 7258. E-mail: vtrajkovic@eunet.yu.

comparison with fullerol and other water-soluble fullerenes. In a subsequent study, the same group reported that the cytotoxic activity of C_{60} colloid was mediated through ROS-mediated cell membrane lipid peroxidation (Sayes *et al.*, 2005). In accordance with these data, a study performed in largemouth bass revealed a significant lipid peroxidation in brains of this aquatic species after 48 h of exposure to underivatized C_{60} (Oberdorster, 2004).

While the markedly higher cytotoxicity of pure C_{60} in comparison with fullerol suggests distinct mechanisms for the induction of cell death, the ability of pure or hydroxylated C_{60} to induce different types of cell death has not been directly compared. Apoptosis and necrosis are two distinct forms of cell death that have profoundly different implications for the surrounding tissues (reviewed in Edinger and Thompson, 2004). Apoptosis is characterized by chromatin condensation, activation of caspases, and fragmentation of DNA without plasma membrane breakdown, followed by packaging of the deceased cell into apoptotic bodies that are recognized and removed by phagocytic cells in the absence of inflammation. On the other hand, necrosis is typified by vacuolation of the cytoplasm, breakdown of the plasma membrane, and release of cellular contents and pro-inflammatory molecules, resulting in the induction of inflammation around the dying cell. Gaining an insight into the type of cell death (apoptotic or necrotic) is important for designing an effective therapeutic strategy against cytotoxins, as apoptosis and necrosis apparently employ different mechanisms for cell killing. For example, inhibition of the apoptotic cascade–initiating enzymes caspases usually blocks apoptosis, while caspase-independent necrosis in some cases can be forestalled by treatment with antioxidants (Edinger and Thompson, 2004).

The toxicity of fullerenes is an important characteristic for defining and constraining their possible biomedical applications, and a complete knowledge of the mechanisms underlying fullerene-induced cell death is necessary for designing an efficient therapeutic strategy for its alleviation. In the present study, we examined the hypothesis that pristine and hydroxylated fullerenes might use distinct mechanisms for the induction of cell death. To that effect, various tests have been employed for analyzing the ability of pure and polyhydroxylated C_{60} to induce apoptotic or necrotic cell death, and to assess the involvement of oxidative stress in the cytotoxicity of the two fullerene-based agents.

MATERIALS AND METHODS

Preparation and characterization of colloid and hydroxylated fullerene. For preparation of fullerene colloid in water, we used a $C_{60/70}$ extract of carbon soot (79% C_{60}, 20% C_{70}, 1% higher-order fullerenes) produced by arc discharge (Markovic *et al.*, 2003). $C_{60/70}$ colloid (referred to as nano-C_{60} for reasons of convenience) was produced by evaporating tetrahydrofuran (THF) from a mixture of water and molecularly dispersed $C_{60/70}$ in THF (Sigma, St. Louis, MO), using the procedure first described by Deguchi *et al.* (2001) and modified by Fortner *et al.* (2005). The concentration of nano-C_{60} suspension in water was adjusted by evaporation to 10 μg/ml, as determined from the absorption spectrum and using a gravimetric procedure. Polyhydroxylated fullerene, referred to as $C_{60}(OH)_n$, was prepared as previously described (Zhao *et al.*, 2004) from the same $C_{60/70}$ extract of carbon soot used for the nano-C_{60} preparation. Immediately after preparation, both nano-C_{60} and $C_{60}(OH)_n$ were transferred to light-protected glass bottles and stored at 4°C until used for experiments. Images of nano-C_{60} were obtained upon evaporation of diluted C_{60} colloid suspension on a 400-mesh carbon-coated copper grid and imaging with a Phillips (FEI Europe B. V., The Netherland) EN 401 transmission electron microscope at 120 kV. The particle size distribution of fullerene colloid was obtained using a Brookhaven Instruments (Holtsville, NY) light-scattering system equipped with a BI-200SM goniometer, a BI-9000AT correlator, a temperature controller, and a Coherent INNOVA 70C argon-ion laser. Dynamic light-scattering measurements were performed using 135 mW laser excitation on 514.5 nm at a 90° detection angle, and particle size distribution was calculated using a Brookhaven Instruments particle-sizing software. For the Fourier transform infrared (FTIR) spectroscopy analysis, nano-C_{60} suspension and $C_{60}(OH)_n$ solution were dried on silicon wafers until thin films were formed. FTIR spectra were measured at room temperature in the spectral range from 400 to 4000 cm^{-1}, on a BOMEM spectrometer.

Cell Lines. The mouse fibrosarcoma cell line L929 was obtained from the European Collection of Animal Cell Cultures (Salisbury, UK), while the rat glioma cell line C6 and the human glioma cell line U251 were kindly donated by Dr Pedro Tranque (Universidad de Castilla-La Mancha, Albacete, Spain). The cell lines were maintained at 37°C in a humidified atmosphere with 5% CO_2, in a HEPES (20mM)–buffered RPMI 1640 cell culture medium (Sigma) supplemented with 5% fetal calf serum, 2mM L-glutamine, 50μM 2-mercaptoethanol, 10mM sodium pyruvate, and 100 IU/ml penicillin and streptomycin (all from Sigma).

Experimental design. The cells were prepared for experiments using the conventional trypsinization procedure with trypsin/EDTA and incubated in flat-bottom 96-well or 6-well cell culture plates (Sarstedt, Newton, NC) for the cell viability assessment or flow cytometry/lipid peroxidation analysis, respectively. Cells (>95% viable, as determined by trypan blue staining) were seeded at a rate of 1×10^4 per well (96-well plates) and 5×10^5 per well (6-well plates) for the short-term treatment (0.5–4 h), or at 0.5×10^4 per well (96-well plates) and 2.5×10^5 per well (6-well plates) for the long-term treatment (18–24 h). After being rested for 18 h, cell cultures were washed to remove the small number of nonadherent dead cells (<5%) and incubated in 200 μl (96-well plates) or 4 ml (6-well plates) of cell culture medium. Cells were incubated alone (control), or treated with fullerenes, antioxidant N-acetylcysteine (NAC), pro-oxidants hydrogen peroxide and 3-morpholinosydnonimine (SIN-1), or pan-caspase inhibitor z-VAD-fmk (all from Sigma), as described in detail in Figures 2–5. To avoid photoexcitation of fullerenes, we tried to minimize their exposure to ambient light, while all cell incubations were performed in the dark. Cells were cultivated under conditions described in the previous section, and cell culture conditions were identical for all cell lines. All treatments in each experiment were performed and analyzed in triplicates, except for the flow cytometry analysis in which single cultures were analyzed. Each experiment was done at least three times.

Determination of cell viability and lactate dehydrogenase release. For the assessment of cell viability, we used the crystal violet assay, which is based on the inability of dead cells to remain adherent to cell culture plastic (Flick and Gifford, 1984). After incubation, cells were washed with PBS to remove dead, nonadherent cells. The remaining adherent, viable cells were fixed with methanol and stained with 1% crystal violet solution at room temperature for 10 min. The plates were thoroughly washed with water, and crystal violet was dissolved in 33% acetic acid. The absorbance of dissolved dye, corresponding to the number of viable cells was measured in an automated microplate reader at 570 nm. The release of intracellular enzyme lactate dehydrogenase (LDH), as a marker of cell membrane damage, was determined exactly as previously

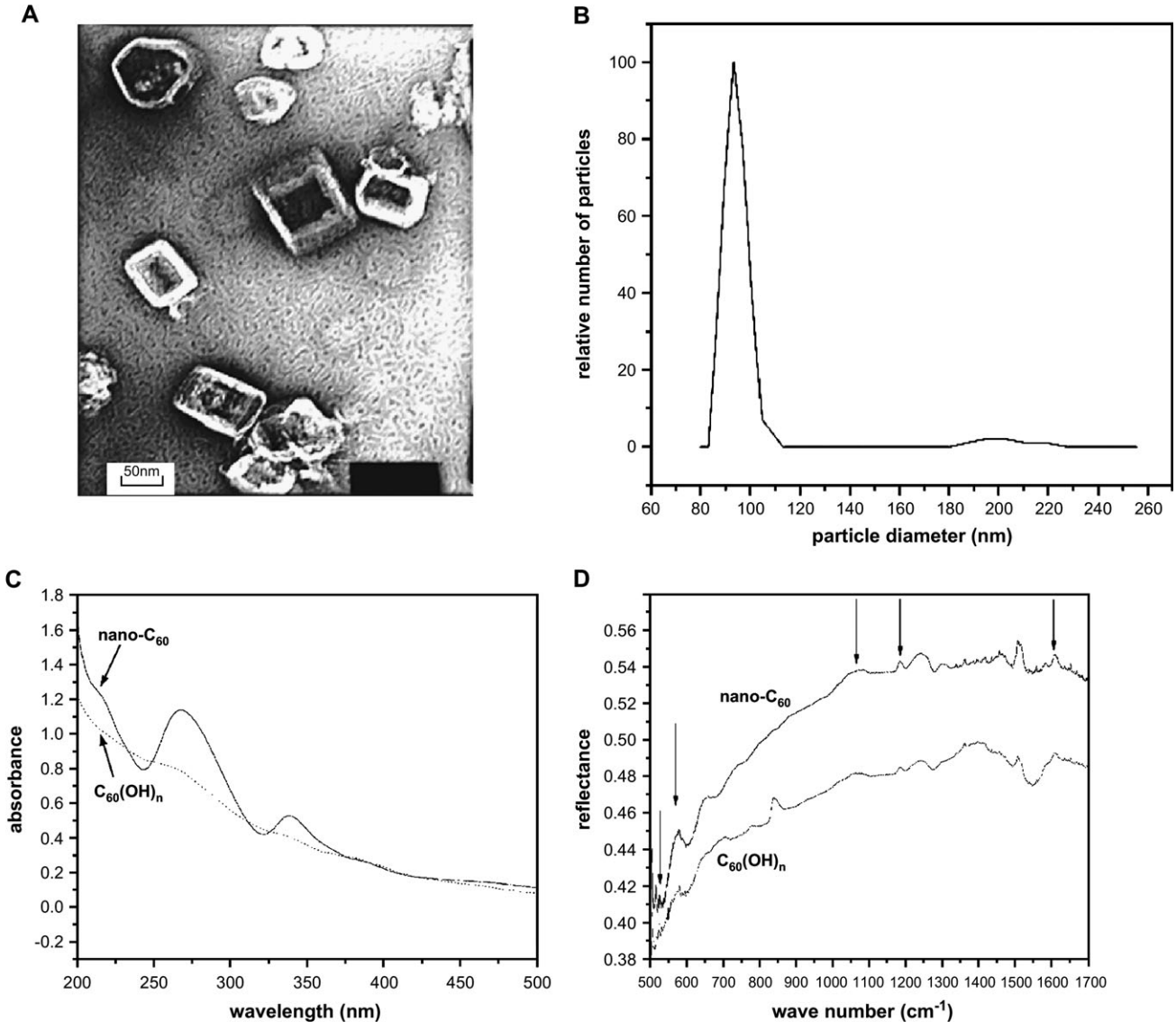

FIG. 1. Characterization of nano-C_{60} and $C_{60}(OH)_n$. (A) Images of nano-C_{60} crystals obtained by transmission electron microscopy. (B) Particle size distribution of nano-C_{60} aggregates in water. Five thousand particles have been analyzed, and the highest number of particles (corresponding to a diameter of 96.3 nm) was normalized to 100. (C) UV/Vis spectra of nano-C_{60} (10 μg/ml) and $C_{60}(OH)_n$ (1000 μg/ml). (D) FTIR spectra of nano-C_{60} and $C_{60}(OH)_n$. The arrows indicate characteristic peaks at 526, 575, 1070, 1182, and 1608 cm^{-1}.

described (Kaludjerovic *et al.*, 2005). The results of both crystal violet and LDH release assays were presented as a percent of the control value obtained in untreated cells.

Detection of apoptosis and necrosis. Apoptotic cell death and necrotic cell death were analyzed by double staining with annexin V–fluorescein isothiocyanate (FITC) and propidium iodide (PI), in which annexin V bound to the apoptotic cells with exposed phosphatidylserine, while PI labeled the necrotic cells with a membrane damage. Staining was performed according to the instructions from the manufacturer (BD Pharmingen, San Diego, CA), and flow cytometry was conducted on a FACSCalibur flow cytometer (BD Pharmingen). DNA fragmentation, another apoptotic marker that is not characteristic for necrotic cells, was assessed by a flow cytometric analysis of ethanol-fixed cells stained with PI as previously described (Kaludjerovic *et al.*, 2005). The percentage of apoptotic (annexin$^+$/PI$^-$ or PI^{low} hypodiploid cells in sub-G_1 fraction) and necrotic (annexin$^+$/PI$^+$) cells was determined using CellQuest Pro software.

Measurement of ROS generation and lipid peroxidation. The production of oxygen radicals was determined by measuring the intensity of green fluorescence emitted by the redox-sensitive dye dihydrorhodamine 123 (DHR) upon excitation at 488 nm. DHR (Sigma) was added to cell cultures 10 min prior to fullerene treatment at a concentration of 1μM. At the end of incubation, cells were detached by trypsinization and washed in PBS, and the fluorescence intensity in treated cells was analyzed using a FACSCalibur flow cytometer with a 488-nm argon laser. Alternatively, DHR fluorescences in nano-C_{60}–treated cell cultures and the cell-free suspension of nano-C_{60} in the cell culture medium were compared using a fluorescence microplate reader (Chameleon, Hidex, Finland) equipped with a 488-nm excitation filter and a 535-nm emission filter. Lipid peroxidation was measured using the colorimetric

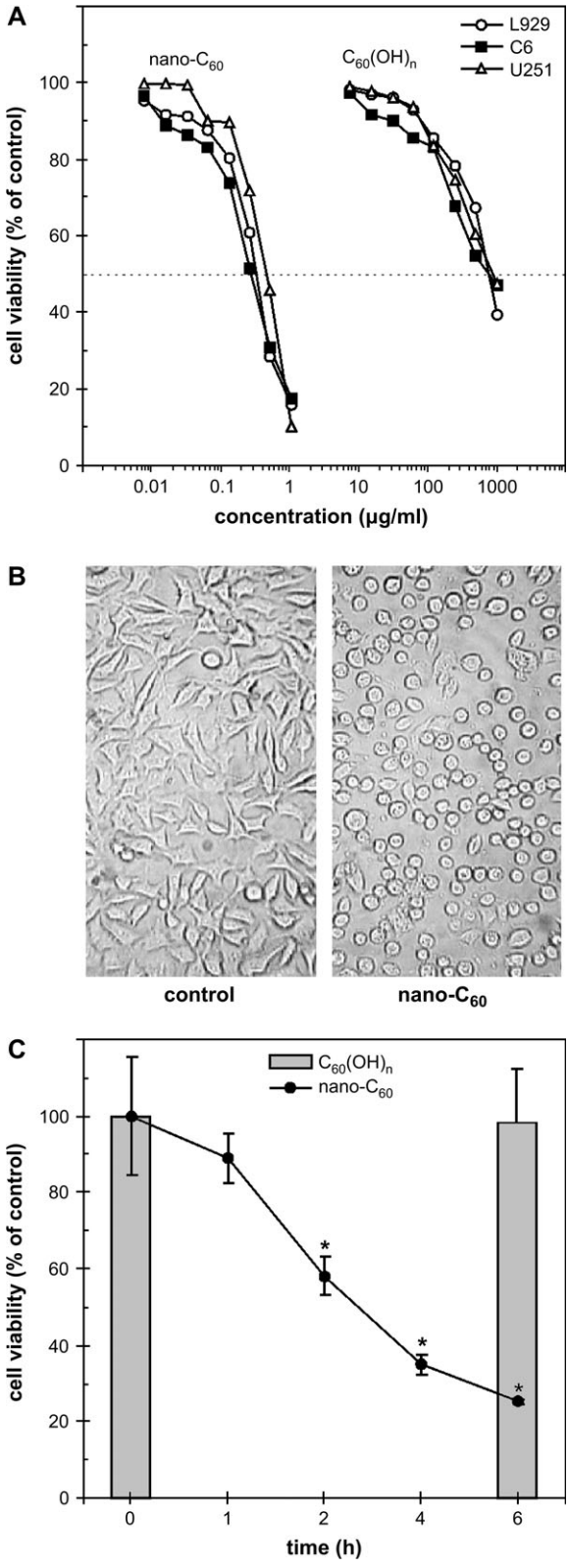

FIG. 2. Different cytotoxic efficiency and kinetics of nano-C_{60} and $C_{60}(OH)_n$. (A) The cells were incubated for 24 h in the absence (control) or presence of nano-C_{60} and $C_{60}(OH)_n$ at different concentrations, and the cell viability was assessed by crystal violet staining. (B) Light micrographs of normal L929 cells (control) and L929 cells exposed to 1 μg/ml nano-C_{60} for 6 h. (C) L929 cells were treated with 1 μg/ml nano-C_{60} (line) or 1000 μg/ml $C_{60}(OH)_n$ (bars), and the cell viability was analyzed by crystal violet assay at the indicated time points (nano-C_{60}) or after 6 h [$C_{60}(OH)_n$] (B). The values in A are means from four independent experiments (SD values were <15% of the corresponding means), while the values in C are mean ± SD of triplicate measurements and are representative of three experiments (*$p < 0.05$).

thiobarbituric acid assay for malondialdehyde (MDA), as previously described (Losa, 2003).

Analysis of synergism and antagonism in cytotoxic interactions. To analyze the type (additive, synergistic, or antagonistic) of fullerene interaction with the pro-oxidant agents H_2O_2 and SIN-1, or the interaction between nano-C_{60} and $C_{60}(OH)_n$ in inducing tumor cell death, cells were treated with each agent alone and in combination. Six twofold dilutions were made from the starting concentrations of 0.5 μg/ml nano-C_{60}, 800 μg/ml $C_{60}(OH)_n$, 1mM H_2O_2, and 1mM SIN-1, and the cytotoxic effect of each dose alone, as well as its combination with the corresponding dose of appropriate agent, was tested using the crystal violet assay. The results were expressed as a percent of cytotoxic efficiency, and a combination index (CI) for mutually exclusive or mutually nonexclusive interactions was calculated according to the method designed by Chou and Talalay (1984). CI values = 1, <1, or >1 indicate additive, synergistic, or antagonistic interactions, respectively.

Statistical analysis. The statistical significance of the observed differences was analyzed by *t*-test or ANOVA followed by the Student-Newman-Keuls test. A p value < 0.05 was considered significant.

RESULTS

Characterization of Nano-C_{60} and $C_{60}(OH)_n$

The images obtained with the transmission electron microscope revealed that C_{60} in water formed nanocrystalline aggregates of approximately 100 nm (Fig. 1A). This is consistent with the results of dynamic light-scattering measurements, which determined the average particle size to be 96.3 nm (Fig. 1B). The dynamic light-scattering analysis of $C_{60}(OH)_n$ showed that all particles were <5 nm (the detection limit), thus confirming the absence of $C_{60}(OH)_n$ aggregation (data not shown). The UV/Vis absorbance spectra of nano-C_{60} and $C_{60}(OH)_n$ in Figure 1C indicate that fullerol does not have pronounced absorption bands in the UV region like nano-C_{60}. Importantly, the spectra of our fullerene preparations are identical to the previously published spectra of similarly prepared commercial C_{60} and $C_{60}(OH)_n$ (Fortner *et al.*, 2005; Vileno *et al.*, 2005). The FTIR spectra of nano-C_{60} and $C_{60}(OH)_n$ show characteristic vibrational modes of C_{60} at 526, 575, and 1182 cm^{-1} (Kuzmany *et al.*, 1995), as indicated by the arrows in Figure 1D. Expectedly, $C_{60}(OH)_n$ has two broad absorption bands at about 1070 and 1608 cm^{-1}, which reflect the presence of C–O and O–H covalent bonds, respectively. However, both bands were also found in the nano-C_{60} spectrum, which is consistent with the data that some degree of derivatization apparently occurs at the surface of nano-C_{60} crystals (Sayes *et al.*, 2005). A strong absorption band at 860 cm^{-1} in the FTIR spectrum of $C_{60}(OH)_n$ is another indication of a C–O bond,

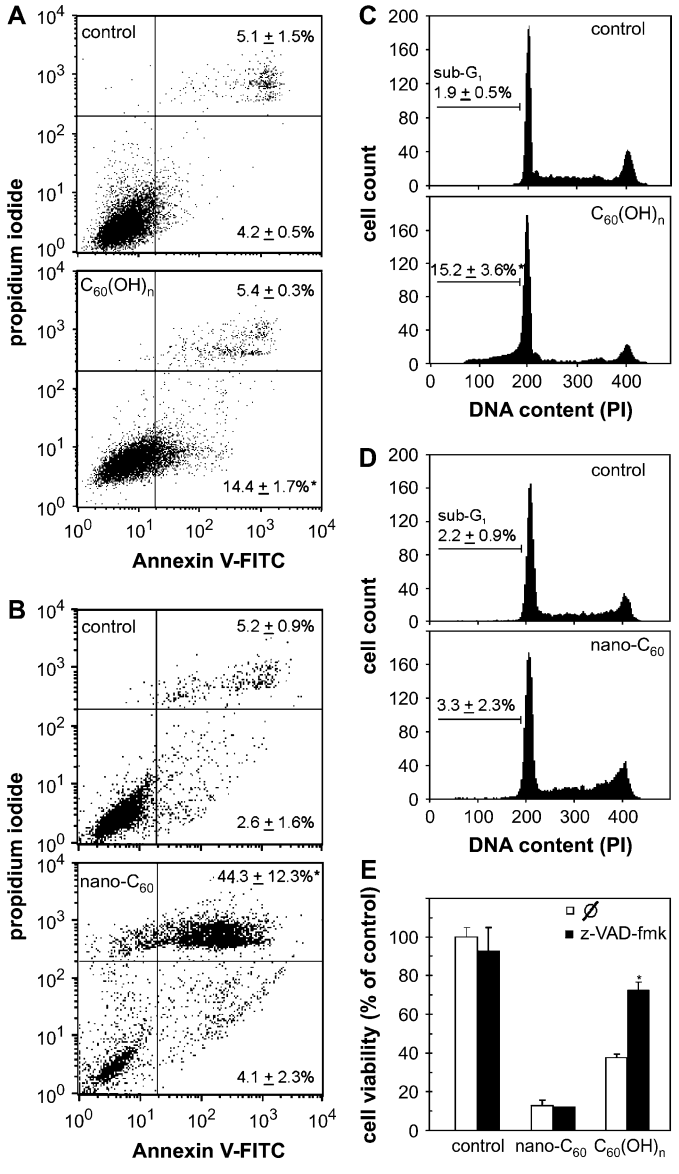

FIG. 3. Pure and hydroxylated C_{60} induce different types of cell death. (A–D) U251 cells were incubated without (control) or with 1000 μg/ml $C_{60}(OH)_n$ for 24 h (A, C) or with 1 μg/ml nano-C_{60} for 6 h (B, D). The number of cells staining with annexin V–FITC and/or PI (A, B), or those with fragmented DNA (PI^{low} sub-G_1 fraction) (C, D), was assessed by flow cytometry. (E) The cytotoxicity of nano-C_{60} (1 μg/ml) and $C_{60}(OH)_n$ (1000 μg/ml) toward U251 cells was investigated after 24-h incubation in the absence or presence of the pan-caspase inhibitor z-VAD-fmk (0.5μM). The values in A–D are means ± SD from three separate experiments, while those in E are mean ± SD of triplicates and are representative of three experiments ($*p < 0.05$).

while the peaks observed in the region between 1200 and 1550 cm^{-1} originate from the silicon substrate.

Nano-C_{60} and $C_{60}(OH)_n$ Differ in the Efficacy and Kinetics of Their Cytotoxic Action

In the preliminary experiments, we used cells of different types and origin (rat primary astrocytes and fibroblasts, rat/mouse peritoneal macrophages, C6 rat astrocytoma, U251 human glioma, and L929 mouse fibrosarcoma cell line) to investigate if fullerenes might exert cell-selective toxicity. However, repeated experiments in which the cell viability after 24-h incubation was evaluated by the crystal violet assay clearly demonstrated that the toxicity of nano-C_{60} and $C_{60}(OH)_n$ was neither species/cell type specific, nor selective for primary or transformed cells (data not shown). Having established that, for reasons of convenience and reproducibility, we used well-defined transformed cell lines (C6, U251, and L929) to delineate the cytotoxic mechanisms of the two different fullerene preparations. To compare the cytotoxic efficiencies of nano-C_{60} and $C_{60}(OH)_n$, different doses of each agent were incubated with the L929, C6, or U251 cell line, and the number of adherent, live cells was assessed by crystal violet staining after 24 h. In accordance with the results of Sayes *et al.* (2005), the data presented in Figure 2A clearly show that pristine fullerene was at least three orders of magnitude more toxic to the tested cell lines than its hydroxylated counterpart [LC_{50} values were 0.25 μg/ml and 800–1000 μg/ml for C_{60} and $C_{60}(OH)_n$, respectively]. Microscopic examination revealed a dramatic change in the morphology of nano-C_{60}–treated cells. In contrast to control cells, nano-C_{60}–treated cells lost their processes and became round and detached from the culture well surface after only 6 h of treatment (Fig. 2B). The observed morphological changes followed by cell detachment were indicative of rapid cell death. Accordingly, the crystal violet analysis of cell viability at various time points following nano-C_{60} addition revealed an extremely fast kinetics of its cytotoxic action, reaching almost maximal efficiency after 6 h of cultivation (Fig. 2C, line). In the same time range, $C_{60}(OH)_n$ failed to cause any discernible changes in cellular morphology (data not shown) or to induce cell death (Fig. 2C, bars). Therefore, pristine C_{60} was a much faster and more efficient cytotoxic agent than its hydroxylated derivative. Importantly, the cytotoxic activity of crystalline C_{60} was completely unrelated to the residual amount (<10% wt/wt) of organic solvent intercalated into its lattice (Sayes *et al.*, 2005), as THF was without any toxic effect (data not shown) even at concentrations 100-fold higher (10 μg/ml) than its estimated residual presence (1 μg/ml nano-C_{60} contains <0.1 μg/ml THF).

Nano-C_{60} and $C_{60}(OH)_n$ Induce Distinct Types of Cell Death

In the following experiments, we compared the ability of nano-C_{60} and $C_{60}(OH)_n$ to induce apoptotic or necrotic cell death. To discriminate between the two distinct types of cell death, we used double staining with annexin V–FITC and PI. Annexin V binds to the phosphatidylserine that is typically exposed at the outer side of cell membrane during apoptosis, while PI only enters the cells with membrane damage that occurs in necrotic cell death. Therefore, normal, healthy cells are $annexin^-/PI^-$ (Fig. 3A, 3B, lower left quadrant), apoptotic cells express phosphatidylserine, but have preserved membrane

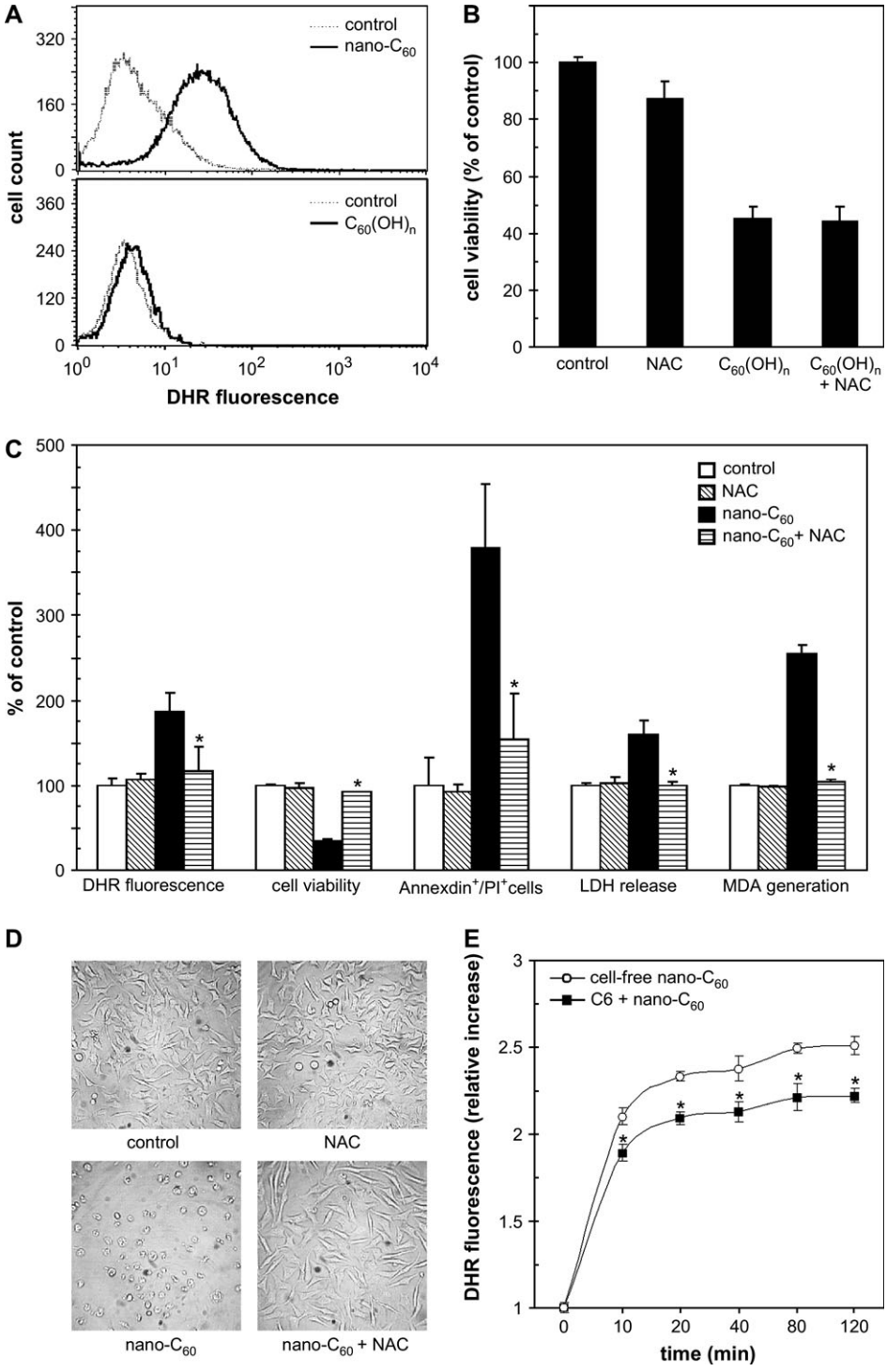

FIG. 4. The involvement of ROS in cytotoxic action of nano-C_{60}. (A) C6 cells were incubated in the absence (control) or presence of nano-C_{60} (1 μg/ml) or $C_{60}(OH)_n$ (1000 μg/ml). The production of ROS was measured by flow cytometric analysis of DHR fluorescence after 3 h (nano-C_{60}) or 18 h [$C_{60}(OH)_n$]. (B) The viability of C6 cells incubated for 24 h without (control) or with $C_{60}(OH)_n$ (1000 μg/ml), in the presence or absence of the antioxidant NAC (2mM). (C) The influence of NAC (2mM) on various parameters determined after exposure of C6 cells to nano-C_{60} (1 μg/ml) for 3 h (DHR, MDA) or 6 h (viability, number of annexin$^+$/PI$^+$ cells, LDH release). (D) Light micrographs of L929 cells incubated for 24 h without (control) or with nano-C_{60} (1 μg/ml), in the presence or absence of NAC (2mM). (E) The ability of nano-C_{60} (1 μg/ml) to generate ROS in C6 cultures and cell-free suspension in cell culture medium was assessed by measuring DHR fluorescence in a microplate reader. The values in B, C, and E are presented as mean ± SD of triplicates and are representative of at least three experiments, with the exception of values for DHR and annexin$^+$/PI$^+$ cells in C, which are means ± SD from three separate experiments (*$p < 0.05$ refers to nano-C_{60} treatment without NAC [C] or the corresponding DHR value obtained in cell-free conditions).

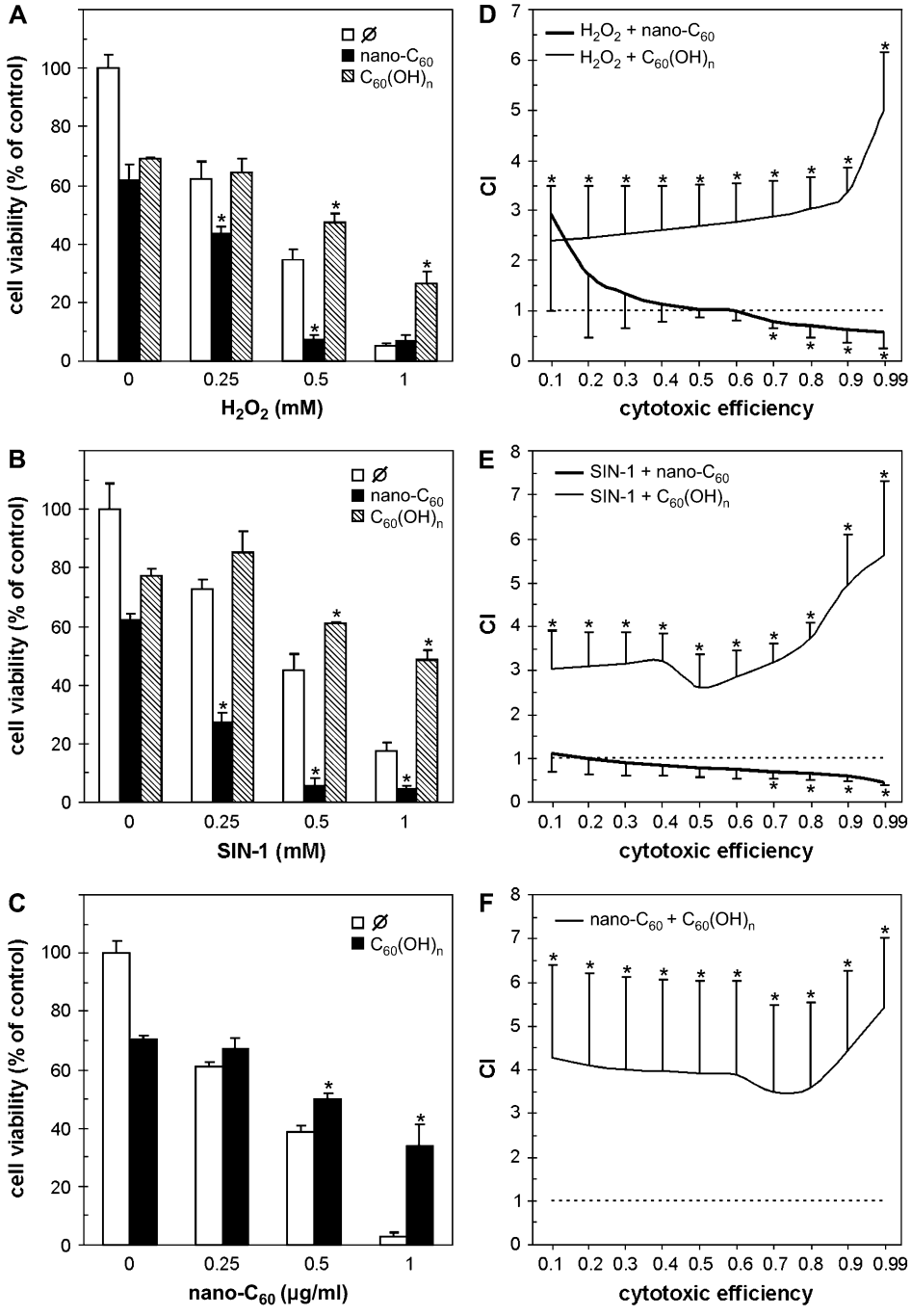

FIG. 5. Hydroxylated C_{60} antagonizes, and nano-C_{60} cooperates with, the cytotoxic action of H_2O_2 and SIN-1. (A, B) Viability of L929 cells exposed for 24 h to various doses of H_2O_2 (A) or SIN-1 (B), in the presence or absence of nano-C_{60} (0.25 μg/ml) or $C_{60}(OH)_n$ (250 μg/ml). (C) Viability of L929 cells treated for 24 h with different concentrations of nano-C_{60}, in the presence or absence of $C_{60}(OH)_n$ (250 μg/ml). (D–F) The interaction of nano-C_{60} and $C_{60}(OH)_n$ with H_2O_2 (D) or SIN-1 (E), as well as the interaction of nano-C_{60} and $C_{60}(OH)_n$ (F) in causing L929 cell death was assessed by Chou-Talalay analysis as described in the "Materials and Methods" section. The results in A–C are presented as mean ± SD of triplicate observations and are representative of at least three experiments, while the CI values in D–F are means ± SD from four separate experiments (*$p < 0.05$ in A–C refers to the corresponding H_2O_2-, SIN-1-, or nano-C_{60}–treated cultures, while *$p < 0.05$ in D–F indicates significant antagonism [CI > 1] or synergism [CI < 1]).

integrity (annexin$^+$/PI$^-$; lower right quadrant), while necrotic cells with damaged membrane stain for both annexin V and PI (annexin$^+$/PI$^+$; upper right quadrant). The results presented in Figures 3A and 3B clearly show that the treatment of U251 cells with $C_{60}(OH)_n$ led to a significant increase in the number of apoptotic, but not necrotic, cells (Fig. 3A), while nano-C_{60} caused a massive increase in the number of necrotic, but not apoptotic, cells (Fig. 3B). The analysis of cellular DNA

content, which is reduced in apoptosis due to DNA fragmentation, was consistent with the data from annexin/PI staining. Namely, the number of hypodiploid, presumably apoptotic, cells with fragmented DNA (sub-G_1 fraction of PI-stained cells) markedly increased upon the treatment of U251 cells with fullerol (Fig. 3C), while pristine fullerene was without effect (Fig. 3D). Similar results were obtained with C6 and L929 cells (data not shown). The ability of nano-C_{60} to cause cell membrane damage indicative of necrosis was also confirmed by a significant increase in LDH release (159 ± 15%, $n = 3$, $p < 0.05$), which was not observed after $C_{60}(OH)_n$ treatment. Due to a difference in the kinetics of cytotoxic action of $C_{60}(OH)_n$ and nano-C_{60} , the assessment of apoptosis/necrosis presented in Figures 3A and 3C and Figures 3B and 3D was performed after 24 and 6 h, respectively. It should be noted, however, that the appearance of annexin$^+$ cells in nano-C_{60}–treated cultures could not be observed even at earlier time points (0.5–4 h; data not shown), which excluded the possibility that some early apoptotic events were overlooked. Finally, we used z-VAD-fmk, a pharmacological inhibitor of caspase activation and subsequent apoptotic cell death, to evaluate the role of apoptosis in fullerene-mediated cytotoxicity. In accordance with the data presented in Figures 3A–3D, z-VAD-fmk exerted a significant protective effect in $C_{60}(OH)_n$-treated U251 cultures, but completely failed to rescue U251 cells from the toxicity of nano-C_{60} (Fig. 3E). Therefore, pure C_{60} and $C_{60}(OH)_n$ apparently employ distinct cytotoxic mechanisms resulting in the preferential induction of caspase-independent necrosis and caspase-dependent apoptosis, respectively.

Cytotoxicity of Nano-C_{60}, but Not $C_{60}(OH)_n$, Depends on ROS Generation

We next investigated the involvement of oxidative stress in the observed cytotoxic action of nano-C_{60} and $C_{60}(OH)_n$. The treatment of C6 cells with $C_{60}(OH)_n$ for 18 h failed to induce detectable intracellular production of ROS, as judged by unaltered intracellular DHR fluorescence (Fig. 4A, lower panel). On the other hand, a considerable increase in DHR fluorescence was observed in C6 cells after 3 h of incubation with pristine C_{60} (Fig. 4A, upper panel), indicating a significant intracellular generation of ROS. It should be noted that a shorter time course was chosen for nano-C_{60} because of the promptness of its cytotoxic action. Nevertheless, the inability of $C_{60}(OH)_n$ to generate ROS was confirmed in the experiments in which the incubation time was reduced from 18 h to 3 or 6 h (data not shown). We used a powerful antioxidant agent, NAC (Zafarullah *et al.*, 2003), to examine the role of ROS production in fullerene-mediated cytotoxicity. While NAC was completely unable to prevent $C_{60}(OH)_n$-mediated tumor cell killing (Fig. 4B), it markedly downregulated the production of oxygen radicals and completely prevented viability loss, induction of necrosis (measured as number of annexin$^+$/PI$^+$ cells), and LDH release associated with nano-C_{60} treatment (Fig. 4C). Moreover, an increase in MDA levels in C6 cells, reflecting membrane lipid peroxidation, was readily observed upon addition of nano-C_{60} and efficiently blocked by NAC treatment (Fig. 4C). The protective effect of NAC was also observed in U251 and L929 cells, and lasted for at least 24 h, as demonstrated by crystal violet staining (data not shown) and the completely preserved morphology of cells treated with nano-C_{60} (Fig. 4D). Because fluorescence-activated cell sorting analysis could not distinguish cell-derived from nano-C_{60}–produced oxygen radicals, we used a fluorescence microplate reader to detect DHR fluorescence in cell-free nano-C_{60} suspension. However, the results presented in Figure 4E show that the time-dependent increase in DHR fluorescence in nano-C_{60}–treated C6 cultures was slightly less pronounced than that observed in the absence of cells. Therefore, it appears that intracellular increase in ROS production was not a cellular response to nano-C_{60} treatment, but rather depended on the ability of pristine fullerene to directly generate oxygen radicals. Collectively, these results suggest that nano-C_{60}–produced oxygen radicals are involved in lipid peroxidation and the consequent necrotic cell death, while $C_{60}(OH)_n$-triggered apoptosis seems to be ROS independent.

Nano-C_{60} and $C_{60}(OH)_n$ Differently Cooperate with the Cytotoxic Action of Oxidative Stress–Inducing Agents

Having demonstrated that the cytotoxicity of nano-C_{60}, but not $C_{60}(OH)_n$, depends on production of oxygen radicals, we wanted to examine if these fullerene preparations could influence the toxicity of other ROS-generating agents. To that effect, we assessed the cytotoxic effects of simultaneous application of nano-C_{60} or $C_{60}(OH)_n$ with hydrogen peroxide and peroxynitrite donor SIN-1, the agents well known for their ability to induce oxidative stress–mediated cell death (Bauer *et al.*, 1998; Wang and Joseph, 1999). In contrast to pristine C_{60}, $C_{60}(OH)_n$ significantly improved the viability of L929 cells treated with H_2O_2 or SIN-1 (Figs. 5A and 5B). We next sought to confirm these observations by using mathematical analysis of drug interaction based on the approach by Chou and Talalay (1984). As shown in Figures 5D and 5E, the CI for combination of $C_{60}(OH)_n$ with H_2O_2 or SIN-1 was > 1 throughout the 0.1–0.99 efficiency range, thus confirming the putative ability of hydroxylated fullerene to antagonize the cytotoxic action of both agents. On the other hand, the CI for combination of nano-C_{60} with H_2O_2 or SIN-1 was around or less than 1 (Figs. 5D and 5E), indicating additive/synergistic cooperation in killing L929 cells. Similar results were obtained with U251 and C6 cells (data not shown). These data suggest that pure C_{60} cooperates with, while its hydroxylated derivative antagonizes, the cytotoxic action of oxidative stress–inducing agents. Interestingly, $C_{60}(OH)_n$ readily antagonized the oxidative stress–dependent cytotoxicity of C_{60} nanocrystals (Figs. 5C and 5F), thus further reinforcing the concept of cell-damaging/pro-oxidant versus

cytoprotective/antioxidant activity of pristine fullerene and its hydroxylated counterpart, respectively.

DISCUSSION

The present study describes the rapid ROS-dependent, caspase-independent necrotic cell death that occurs within only few hours of exposure to pure buckminsterfullerene aggregates (nano-C_{60}). On the other hand, polyhydroxylated C_{60} caused delayed, ROS-independent, caspase-mediated apoptosis. It should be noted that the observed toxic effects were not restricted to the transformed cell lines, as similar results were obtained in primary rat astrocytes and fibroblasts, as well as in rat and mouse peritoneal macrophages (Isakovic *et al.*, unpublished observation).

While cytotoxic/antiproliferative effects of pristine C_{60} and its various water-soluble derivatives, including $C_{60}(OH)_n$, have been observed in different experimental systems (Bogdanovic *et al.*, 2004; Bosi *et al.*, 2004; Chen *et al.*, 2004; Lu *et al.*, 1998; Mashino *et al.*, 2003; Sayes *et al.*, 2004, 2005; Tsuchiya *et al.*, 1996; Yang *et al.*, 2002), their capacity for preferential induction of apoptosis or necrosis has not been compared. Although the release of LDH observed after 48-h incubation of human dermal fibroblasts, astrocytes, or liver carcinoma cells with nano-C_{60} (Sayes *et al.*, 2005) is consistent with necrotic cell death, secondary necrosis following an initially apoptotic death could not be excluded. A line of evidence from the present study, including the results of cell membrane asymmetry/integrity assessment by annexin V/PI staining or LDH release test, as well as the data from DNA fragmentation analysis, clearly demonstrate that cell death induced by nano-C_{60} and $C_{60}(OH)_n$ proceeds exclusively through the necrotic and apoptotic pathways, respectively. Since aspartate-specific cysteine proteases, termed caspases, are apparently required for apoptotic, but not necrotic, cell death (Ferrari *et al.*, 1999; Los *et al.*, 2002), the protective effect of caspase inhibition in $C_{60}(OH)_n$-treated cells, but not C_{60}-treated cells, further supports the view that pristine fullerene induces necrotic cell death, as opposed to the mainly pro-apoptotic activity of its hydroxylated derivative. The mode of cell death might profoundly influence the healing of the surrounding tissue, since necrotic cell products could initiate additional injury by promoting inflammation (Jaeschke *et al.*, 2002). On the other hand, in view of the immunostimulatory properties of necrotic cells and resistance of tumor cells to apoptosis, it has been proposed that necrosis might be more efficient than apoptosis in inducing tumor regression (Edinger and Thompson, 2004; Galluci *et al.*, 1999; Reiter *et al.*, 1999). Therefore, the ability to rapidly induce necrotic, rather than apoptotic, cell death could pose a difficulty for counteracting the toxicity of nanocrystalline C_{60}, as well as potentially increase its efficiency in cancer therapy.

By using the redox-sensitive fluorescent dye DHR, MDA measurement, and cell incubation with the well-known antioxidant agent NAC, we have shown that nano-C_{60}–induced necrosis was exclusively a consequence of oxidative stress that probably resulted in lipid peroxidation–mediated damage of the cell membrane. The putative involvement of oxygen radicals in nano-C_{60}–induced necrosis is consistent with the ability of another antioxidant, L-ascorbic acid, to completely prevent lipid peroxidation and ensuing cell death in nano-C_{60}–treated cultures of human dermal fibroblasts, described recently by Sayes *et al.* (2005). Based on their observation that C_{60} nanocrystals generate superoxide anions in a cell-free system (Sayes *et al.*, 2004), the authors assumed that this feature of nano-C_{60} could be solely responsible for the induction of oxidative stress and subsequent cell death. However, it was not possible to conclude from these studies whether the target cells contributed to production of oxygen radicals in response to treatment with pure C_{60}. By comparing the nano-C_{60}–evoked increase in DHR fluorescence in tumor cell cultures and cell-free solution, we have been able to provide some direct evidence in support of the hypothesis by Sayes *et al.* (2004), as the cells themselves apparently did not contribute to ROS generation in our experiments. Moreover, we have demonstrated a slight, but significant, decrease in the ability of nano-C_{60} to generate oxygen radicals in the presence of cells, which might be a consequence of the cellular antioxidative defense. Indeed, it has been shown that cells increase their production of antioxidant glutathione in response to oxidative stress induced by exposure to pristine C_{60} (Sayes *et al.*, 2005). However, it still remains to be established if ROS production and subsequent damage were limited to cell membrane, or nano-C_{60} could somehow gain access to the cell cytoplasm.

In contrast to nano-C_{60}–triggered necrosis, apoptosis induced by $C_{60}(OH)_n$ proceeded entirely in a ROS-independent fashion. Furthermore, $C_{60}(OH)_n$ significantly antagonized the cytotoxic action of the oxidative stress–inducing agents H_2O_2 and peroxynitrite donor SIN-1, as demonstrated by the Chou-Talalay approach. This is consistent with the previously reported ability of $C_{60}(OH)_n$ to prevent oxidative stress and subsequent cell death in various experimental settings (Chen *et al.*, 2004; Dugan *et al.*, 1996; Jin *et al.*, 2000; Murugan *et al.*, 2002; Tsai *et al.*, 1997), supporting a general view that $C_{60}(OH)_n$ mainly acts as a ''free radical sponge'' with only mild cytotoxic activity (Bosi *et al.*, 2003). On the other hand, the present study confirmed the recently described capacity of nanocrystalline C_{60} to generate oxygen radicals in cell-free systems (Sayes *et al.*, 2004), while extending this observation by demonstrating ROS production in nano-C_{60}–treated cells. This pro-oxidant activity might account for our novel finding that pristine C_{60}, in contrast to its hydroxylated derivative, readily cooperated in a synergistic fashion with H_2O_2 and peroxynitrite in the induction of cell death. It seems conceivable to assume that the mechanisms underlying the pro- versus antioxidant effects of pristine and hydroxylated fullerene might be related to differences in their chemical structures. Namely, the transmission electron microscopy images and light-scattering measurements

obtained in the present study confirm that a substantial fraction of pristine C_{60}, unlike the fullerene core in intentionally water-solubilized derivatives, is contained in the interior of the nanocrystalline aggregates of approximately 90–100 nm in size (Fortner *et al.*, 2005; Sayes *et al.*, 2004). As a consequence, C_{60} in such conditions remains largely underivatized (>99%), and its high toxicity is therefore consistent with the finding that ROS generation and cytotoxicity decrease with increasing derivatization of the fullerene cage (Sayes *et al.*, 2004). However, it remains to be revealed how this structural difference could lead to distinct oxidant and cytotoxic properties. To further emphasize the complexity of the oxidant behavior of fullerenes in biological systems, we note that even polyhydroxylated fullerenes could generate oxygen radicals under certain circumstances (e.g., upon photosensitization) (Kamat *et al.*, 1998, 2000). On the other hand, the ability of nano-C_{60} to produce ROS does not seem to depend on the presence of light (Sayes *et al.*, 2004), which is consistent with our results that exposure to visible light or UV did not affect the cytotoxicity of nano-C_{60} (unpublished data).

In contrast to the mainly antioxidant/cytoprotective and only mild ROS-independent pro-apoptotic activity of polyhydroxylated C_{60}, the present study clearly demonstrates the ability of pure crystalline C_{60} to induce rapid ROS-dependent necrosis and to synergistically enhance the cytotoxicity of other oxidative stress–inducing agents. This is consistent with a recent study in which the presence of pristine C_{60} in water caused lipid peroxidation–mediated damage to fish brain (Oberdorster, 2004), but the possible relevance of our findings for the *in vivo* toxicity of nano-C_{60} is still to be investigated. While the difference in the cytotoxic mechanisms of pure versus hydroxylated C_{60} suggests distinct remediation for their unwarranted biological effects, their divergent cytotoxic/cytoprotective properties also provide grounds for the development of fullerenes as either cytoprotective or anticancer therapeutics.

ACKNOWLEDGMENTS

This work was supported by the Ministry of Science and Environmental Protection of the Republic of Serbia (Grant No. 145073). We thank Natasa Bibic (Vinca Institute of Nuclear Sciences, Belgrade) for performing transmission electron microscopy, Nebojsa Romcevic (Institute of Physics, Belgrade) for the FTIR analysis, and Marija Mostarica Stojkovic and Zorica Ramic (Institute of Microbiology and Immunology, School of Medicine, Belgrade) for helpful discussion.

REFERENCES

Bauer, M. K., Vogt, M., Los, M., Siegel, J., Wesselborg, S., and Schulze-Osthoff, K. (1998). Role of reactive oxygen intermediates in activation-induced CD95 (APO-1/Fas) ligand expression. *J. Biol. Chem.* **273,** 8048–8055.

Bogdanovic, G., Kojic, V., Dordevic, A., Canadanovic-Brunet, J., Vojinovic-Miloradov, M., and Baltic, V. V. (2004). Modulating activity of fullerol $C_{60}(OH)_{22}$ on doxorubicin-induced cytotoxicity. *Toxicol. In Vitro* **18,** 629–637.

Bosi, S., Da Ros, T., Spalluto, G., and Prato, M. (2003). Fullerene derivatives: An attractive tool for biological applications. *Eur. J. Med. Chem.* **38,** 913–923.

Bosi, S., Feruglio, L., Da Ros, T., Spalluto, G., Gregoretti, B., Terdoslavich, M., Decorti, G., Passamonti, S., Moro, S., and Prato, M. (2004). Hemolytic effects of water-soluble fullerene derivatives. *J. Med. Chem.* **47,** 6711–6715.

Chen, Y. W., Hwang, K. C., Yen, C. C., and Lai, Y. L. (2004). Fullerene derivatives protect against oxidative stress in RAW 264.7 cells and ischemia-reperfused lungs. *Am. J. Physiol. Regul. Integr. Comp. Physiol.* **287,** R21–R26.

Cheng, X., Kan, A. T., and Tomson, M. B. (2004). Naphthalene adsorption and desorption from aqueous C_{60} fullerene. *J. Chem. Eng. Data* **49,** 675–683.

Chou, T. C., and Talalay, P. (1984). Quantitative analysis of dose-effect relationships: The combined effects of multiple drugs or enzyme inhibitors. *Adv. Enzyme Regul.* **22,** 27–55.

Deguchi, S., Rossitza, G. A., and Tsujii, K. (2001). Stable dispersions of fullerenes, C_{60} and C_{70} in water. Preparation and characterization. *Langmuir* **17,** 6013–6017.

Dugan, L. L., Gabrielsen, J. K., Yu, S. P., Lin, T. S., and Choi, D. W. (1996). Buckminsterfullerenol free radical scavengers reduce excitotoxic and apoptotic death of cultured cortical neurons. *Neurobiol. Dis.* **3,** 129–135.

Dugan, L. L., Lovett, E. G., Quick, K. L., Lotharius, J., Lin, T. T., and O'Malley, K. L. (2001). Fullerene-based antioxidants and neurodegenerative disorders. *Parkinsonism Relat. Disord.* **7,** 243–246.

Dugan, L. L., Turetsky, D. M., Du, C., Lobner, D., Wheeler, M., Almli, C. R., Shen, C. K., Luh, T. Y., Choi, D. W., and Lin, T. S. (1997). Carboxyfullerenes as neuroprotective agents. *Proc. Natl. Acad. Sci. U.S.A.* **94,** 9434–9439.

Edinger, A. L., and Thompson, C. B. (2004). Death by design: Apoptosis, necrosis and autophagy. *Curr. Opin. Cell Biol.* **16,** 663–669.

Ferrari, D., Los, M., Bauer, M. K., Vandenabeele, P., Wesselborg, S., and Schulze-Osthoff, K. (1999). P2Z purinoreceptor ligation induces activation of caspases with distinct roles in apoptotic and necrotic alterations of cell death. *FEBS Lett.* **447,** 71–75.

Flick, D. A., and Gifford, G. E. (1984). Comparison of in vitro cell cytotoxic assays for tumor necrosis factor. *J. Immunol. Methods* **68,** 167–175.

Fortner, J. D., Lyon, D. Y., Sayes, C. M., Boyd, A. M., Falkner, J. C., Hotze, E. M., Alemany, L. B., Tao, Y. J., Guo, W., Ausman, K. D., *et al.* (2005). C_{60} in water: Nanocrystal formation and microbial response. *Environ. Sci. Technol.* **39,** 4307–4316.

Galluci, S., Lolkema, M., and Matzinger, P. (1999). Natural adjuvants: Endogenous activators of dendritic cells. *Nat. Med.* **5,** 1249–1255.

Jaeschke, H., Gores, G. J., Cederbaum, A. I., Hinson, J. A., Pessayre, D., and Lemasters, J. J. (2002). Mechanisms of hepatotoxicity. *Toxicol. Sci.* **65,** 166–176.

Jin, H., Chen, W. Q., Tang, X. W., Chiang, L. Y., Yang, C. Y., Schloss, J. V., and Wu, J. Y. (2000). Polyhydroxylated C_{60}, fullerenols, as glutamate receptor antagonists and neuroprotective agents. *J. Neurosci. Res.* **62,** 600–607.

Kaludjerovic, G., Miljkovic, D., Momcilovic, M., Djinovic, V., Mostarica Stojkovic, M., Sabo, T., and Trajkovic, V. (2005). Novel platinum complexes induce rapid tumor cell death in vitro. *Int. J. Cancer* **116,** 479–486.

Kamat, J. P., Devasagayam, T. P., Priyadarsini, K. I., and Mohan, H. (2000). Reactive oxygen species mediated membrane damage induced by fullerene derivatives and its possible biological implications. *Toxicology* **155,** 55–61.

Kamat, J. P., Devasagayam, T. P., Priyadarsini, K. I., Mohan, H., and Mittal, J. P. (1998). Oxidative damage induced by the fullerene C_{60} on photosensitization in rat liver microsomes. *Chem-Biol. Interact.* **114,** 145–159.

Kuzmany, H., Winkler, R., and Pichler, T. (1995). Infrared spectroscopy of fullerenes. *J. Phys. Condens. Matter* **7,** 6601–6624.

Los, M., Mozoluk, M., Ferrari, D., Stepczynska, A., Stroh, C., Renz, A., Herceg, Z., Wang, Z. Q., and Schulze-Osthoff, K. (2002). Activation and caspase-mediated inhibition of PARP: A molecular switch between fibroblast necrosis and apoptosis in death receptor signaling. *Mol. Biol. Cell* **13,** 978–988.

Losa, G. A. (2003). Resveratrol modulates apoptosis and oxidation in human blood mononuclear cells. *Eur. J. Clin. Investig.* **33,** 818–823.

Lotharius, J., Dugan, L. L., and O'Malley, K. L. (1999). Distinct mechanisms underlie neurotoxin-mediated cell death in cultured dopaminergic neurons. *J. Neurosci.* **19,** 1284–1293.

Lu, L. H., Lee, Y. T., Chen, H. W., Chiang, L. Y., and Huang, H. C. (1998). The possible mechanisms of the antiproliferative effect of fullerenol, polyhydroxylated C_{60}, on vascular smooth muscle cells. *Br. J. Pharmacol.* **123,** 1097–1102.

Markovic, Z., Todorovic-Markovic, B., Marinkovic, M., and Nenadovic, T. (2003). Temperature measurement of carbon arc plasma in helium. *Carbon* **41,** 369–371.

Mashino, T., Nishikawa, D., Takahashi, K., Usui, N., Yamori, T., Seki, M., Endo, T., and Mochizuki, M. (2003). Antibacterial and antiproliferative activity of cationic fullerene derivatives. *Bioorg. Med. Chem. Lett.* **13,** 4395–4397.

Murugan, M. A., Gangadharan, B., and Mathur, P. P. (2002). Antioxidative effect of fullerenol on goat epididymal spermatozoa. *Asian J. Androl.* **4,** 149–152.

Oberdorster, E. (2004). Manufactured nanomaterials (fullerenes, C_{60}) induce oxidative stress in the brain of juvenile largemouth bass. *Environ. Health Perspect.* **112,** 1058–1062.

Reiter, I., Krammer, G., and Schwamberger, G. (1999). Differential effect of apoptotic versus necrotic tumor cells on macrophage antitumour activity. *J. Immunol.* **163,** 1730–1732.

Sayes, C., Fortner, J., Lyon, D., Boyd, A., Ausman, K., Tao, Y., Sitharaman, B., Wilson, L., West, J., and Colvin, V. L. (2004). The differential cytotoxicity of water soluble fullerenes. *Nano Lett.* **4,** 1881–1887.

Sayes, C. M., Gobin, A. M., Ausman, K. D., Mendez, J., West, J. L., and Colvin, V. L. (2005). Nano-C_{60} cytotoxicity is due to lipid peroxidation. *Biomaterials* **26,** 7587–7595.

Tsai, M. C., Chen, Y. H., and Chiang, L. Y. (1997). Polyhydroxylated C_{60}, fullerenol, a novel free-radical trapper, prevented hydrogen peroxide- and cumene hydroperoxide-elicited changes in rat hippocampus in vitro. *J. Pharm. Pharmacol.* **49,** 438–445.

Tsuchiya, T., Oguri, I., Yamakoshi, Y. N., and Miyata, N. (1996). Novel harmful effects of [60]fullerene on mouse embryos in vitro and in vivo. *FEBS Lett.* **393,** 139–145.

Vileno, B., Lekka, M., Sienkiewicz, A., Marcoux, P., Kulik, A. J., Kasas, S., Catsicas, S., Graczyk, A., and Forro, L. (2005). Singlet oxygen [(1)Delta(g)]-mediated oxidation of cellular and subcellular components: ESR and AFM assays. *J. Phys. Condens. Matter* **17,** S1471–S1482.

Wang, H., and Joseph, J. A. (1999). Quantifying cellular oxidative stress by dichlorofluorescein assay using microplate reader. *Free Radic. Biol. Med.* **27,** 612–616.

Yang, X. L., Fan, C. H., and Zhu, H. S. (2002). Photo-induced cytotoxicity of malonic acid [C_{60}]fullerene derivatives and its mechanism. *Toxicol. In Vitro* **16,** 41–46.

Zafarullah, M., Li, W. Q., Sylsvester, J., and Ahmad, M. (2003). Molecular mechanisms of N-acetylcysteine actions. *Cell. Mol. Life Sci.* **60,** 6–20.

Zhao, G. C., Zhang, P., Wei, X. W., and Yang, Z. S. (2004). Determination of proteins with fullerol by a resonance light scattering technique. *Anal. Biochem.* **334,** 297–302.